Three-component hybrid-integrated optical accelerometer based on $LiNbO_3$ photoelastic waveguide

Donglin Tang (唐东林)*, Zheng Liang (梁 政), Xiaodong Zhang (张晓东), Shan He (何 山), and Feng Guo (郭 峰)

Faculty of Mechanical and Electronic Engineering, Southwest Petroleum University, Key Laboratory of Petroleum-Gas Equipment, Ministry of Education of China, Chengdu 610500

**E-mail: xnsytdl@yahoo.com.cn*

Received February 27, 2008

A novel three-component hybrid-integrated optical accelerometer based on $LiNbO_3$ photoelastic waveguide is presented. The photoelasitcity of $LiNbO_3$ due to three-dimensional stress states is obtained analytically. We analyze the level of sensitivity to cross-axis accelerations which is a very important parameter for three-component accelerometer. Theoretically, the designed three-component hybrid-integrated optical accelerometer has a transverse sensitivity ratio (TSR) of zero. The sensor has a high natural frequency of 3.5 kHz and a linear broad working frequency.

OCIS codes: 130.6010, 280.4788.
doi: 10.3788/COL20090701.0032.

Optical fiber sensor has been widely used to detect acceleration in virtue of its wide bandwidth, long-distance transmission, and immunity to electromagnetic interference in optical fiber[1−6]. Integrated optical sensors using single-mode waveguides are more compact, stable, and physically robust and may be more easily fabricated by mass production techniques than those using discrete optical components[7−10].

In this letter, on the basis of the previous work on Michelson fiber-optic accelerometer[11,12], we present a novel three-component hybrid-integrated optical accelerometer based on $LiNbO_3$ photoelastic effect. Polarizers and phase modulators are integrated with the Mach-Zehnder interferometer (MZI) fabricated by integrated optics technology on $LiNbO_3$ substrate. The resonant frequency of the accelerometer is 3.5 kHz. It can be employed to monitor or accurately measure vibrations in various areas such as seismic measurement in geophysical survey etc.

We use the one-dimensional accelerometer to explain the operating principle of the three-component photoelastic waveguide accelerometer. The MZI on the X-cut Y-propagation $LiNbO_3$ substrate (the light axis is along the Z direction) is shown in Fig. 1. Using the technology of integrated optics, branch-waveguide can be fabricated so as to integrate light and split light on the $LiNbO_3$ substrate. The horizontally polarized laser beam from a laser diode (LD) with the output intensity I at the wavelength λ passes through a horizontal polarizer to assure that the beam is polarized perpendicular to the stress direction caused by acceleration forces on proof mass. After passing through the polarizer, the beam is divided by symmetric Y-branch waveguide, resulting in two separate beams with intensity of $I/2$ traveling in respective waveguides. The beams are further split by symmetric Y-branch waveguides, forming four separate beams traveling in four waveguides with intensity of $I/4$. When the proof mass is accelerated with acceleration forces in the direction of ΔF, it will stress one waveguide in tension and the other in compression, changing the refraction index of the photoelastic waveguides. The phase shift following the variation of the index will be adjusted by external acceleration. The light beams passing through the waveguides, which are not stressed, pass through two 90° phase bias elements, respectively. The light beams modulated by external acceleration and phase modulator will pass through polarizers after being coupled by the branch waveguide. The polarizers are employed to realize and maintain the polarization state of the output lightwave, and filtrate the optical signal out of detection directions. The light signal is converted to an electrical signal by photo-detectors. We will get the acceleration by dealing with the electrical signal which is fed into the signal processor unit. The acceleration a_k acting on the

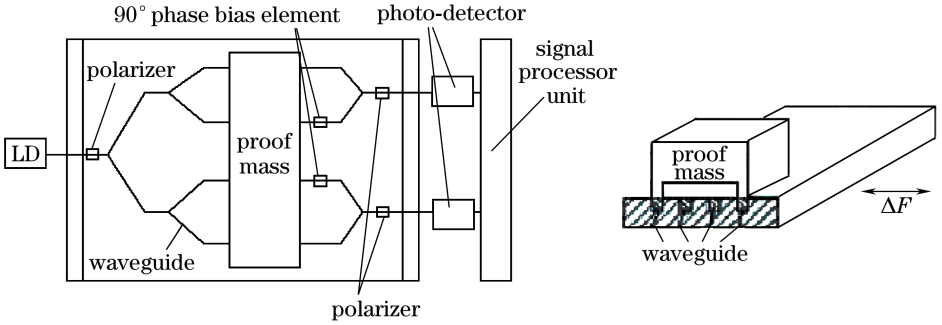

Fig. 1. Hybrid-integrated optic chip for acceleration detection.

1671-7694/2009/010032-04

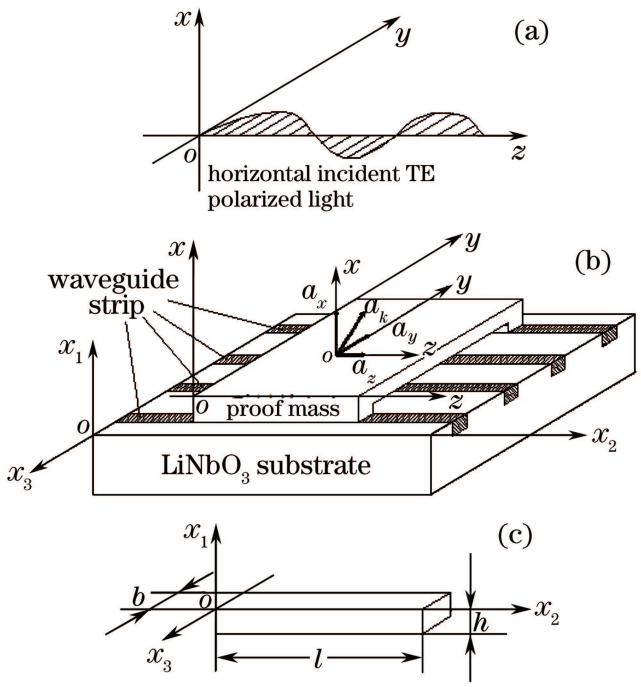

Fig. 2. Photoelastic effect due to the three-dimensional acceleration. (a) Horizontal TE polarized light incident on the proof mass; (b) analysis model; (c) proof mass under acceleration.

proof mass in any direction can be resolved into a_x, a_y, and a_z, where polarized light is traveling along the axes shown in Fig. 2.

If the optical phase shift caused by three-dimensional acceleration is $\Delta\phi_m$, the change of index corresponding to the optical phase shift is

$$\Delta n_m = \frac{\lambda}{2\pi l}\Delta\phi_m, \tag{1}$$

where $\lambda = 1.3$ μm; the waveguide dimensions of the sensor are length $l = 10$ mm, width $b = 6.5$ μm, height $h = 2.5$ μm; the proof mass $m = 50$ g; the indices of light axis for o- and e-light are $n_{\rm o} = 2.219$, $n_{\rm e} = 2.145$.

According to $LiNbO_3$ photoelastic effect, we get the relationship between the change of optical phase and the three-dimensional acceleration of our sensor, which can be rewritten as

$$\begin{pmatrix} (2.07\times10^{-5}\Delta\phi_x + 2.219)^2 - 0.20 \\ (2.07\times10^{-5}\Delta\phi_y + 2.219)^2 - 0.20 \\ (2.07\times10^{-5}\Delta\phi_z + 2.145)^2 - 0.22 \end{pmatrix}$$

$$= \begin{pmatrix} -0.057\times10^{-6} & 0.55\times10^{-6} & 0.88\times10^{-3} \\ -0.198\times10^{-6} & -0.24\times10^{-6} & 0.88\times10^{-3} \\ 0.29\times10^{-6} & 0.9\times10^{-6} & -0.03\times10^{-3} \end{pmatrix}$$

$$\times \begin{pmatrix} a_x + g \\ a_y \\ a_z \end{pmatrix}. \tag{2}$$

Thus we can obtain the total acceleration:

$$a = \sqrt{a_x^2 + a_y^2 + a_z^2}. \tag{3}$$

The important characteristic of three-component accelerometer is transverse sensitivity ratio (TSR), which is defined as the ratio of cross-axis sensitivity $K_{\rm cross-axis}$ to on-axis sensitivity $K_{\rm on-axis}$ of accelerometer. If the noise of three-component accelerometer is large or the on-axis sensitivity is small, the TSR is large. As the three-component accelerometer we designed, the proof mass attached to the photoelastic waveguide is differentially responsive to acceleration force to stress waveguides and causes a phase difference between the stressed and unstressed waveguide beams. This phase difference is proportional to input acceleration, so we can get the phase sensitivity as

$$K_{\rm on-axis} = \frac{\Delta\phi_{\rm on-axis}}{\Delta a_{\rm on-axis}}, \quad K_{\rm cross-axis} = \frac{\Delta\phi_{\rm cross-axis}}{\Delta a_{\rm on-axis}},$$

$$\mathrm{TSR} = \frac{K_{\rm cross-axis}}{K_{\rm on-axis}}. \tag{4}$$

Hybrid-integrated optical three-component accelerometers with different structures have different sensitivities and TSRs. We can get different TSR values of different structures from Eqs. (2) and (4), and choose a more suitable structure.

We have studied TSRs of accelerometers with combined structure and integrated structure, respectively. Figure 3 shows a schematic diagram of the harmonic vibrator of the combined three-component photoelastic waveguide accelerometer. It consists of three separated dual MZIs on X-cut and Y-propagation $LiNbO_3$, respectively. With the separated dual MZIs fixed on a body, a harmonic vibrator of the combined three-component photoelastic waveguide accelerometer is designed. For the integrated structure, three separated dual MZIs are monolithically integrated on three vertical surfaces of an X-cut and Y-propagation $LiNbO_3$ crystal respectively, as shown in Fig. 4.

Substituting the design parameters into Eqs. (2) and (4), we get TSR and cross-axis sensitivity due to the acceleration of different directions, as shown in Table 1. The TSR value in the combined structure is 0, whereas the minimum TSR value in the integrated structure is 0.19. Considering the analysis above, we employ the combined structure to design the accelerometer.

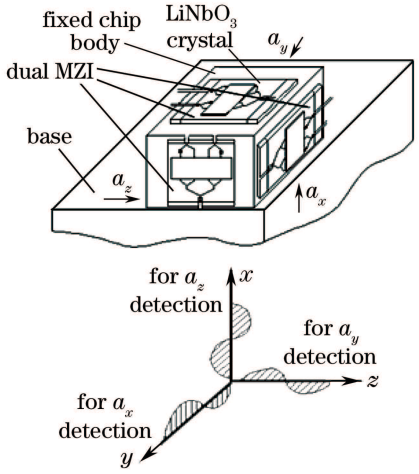

Fig. 3. Harmonic vibrator of the combined three-component photoelastic waveguide accelerometer.

Table 1. TSR in the Three-Component Photoelastic Waveguide Accelerometer

Structure	a_z		a_x		a_y	
	$K_{\mathrm{cross-axis}}$ (rad/(m/s^2))	TSR	$K_{\mathrm{cross-axis}}$ (rad/(m/s^2))	TSR	$K_{\mathrm{cross-axis}}$ (rad/(m/s^2))	TSR
Integrated	$K_{\mathrm{cross-axis}_y} = K_{\mathrm{cross-axis}_x}$ $= \frac{2\pi}{\lambda} n_o^3 p_{13} \times 7.73 \times 10^{-3}$	TSR_x $= \mathrm{TSR}_y$ $= 1.87 \frac{n_o^3}{n_e^3}$	$K_{\mathrm{cross-axis}_y} = 463.3$, $K_{\mathrm{cross-axis}_z} = 306.2$	TSR_y, $= 0.28$ TSR_z $= 0.19$	$K_{\mathrm{cross-axis}_x} = 166.9$, $K_{\mathrm{cross-axis}_x} = 98.6$	$\mathrm{TSR}_x = 0.43$, $\mathrm{TSR}_z = 0.25$
Combined	$K_{\mathrm{cross-axis}} = 0$, $\mathrm{TSR} = \frac{K_{\mathrm{cross-axis}}}{K_{\mathrm{primary-axis}}} = \frac{0}{\frac{2\pi}{\lambda} \Delta n_e p_{33} \times 7.73 \times 10^{-3}} = 0$					

p_{13} and p_{33} are photoelastic constants of $LiNbO_3$ crystal. TSR_x, TSR_y, and TSR_z are transverse sensitivity ratios of x, y, z axes, respectively.

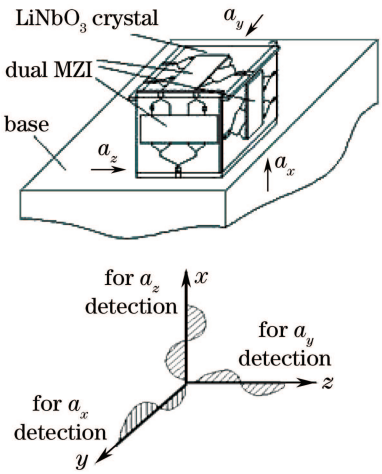

Fig. 4. Harmonic vibrator of the integrated three-component photoelastic waveguide accelerometer.

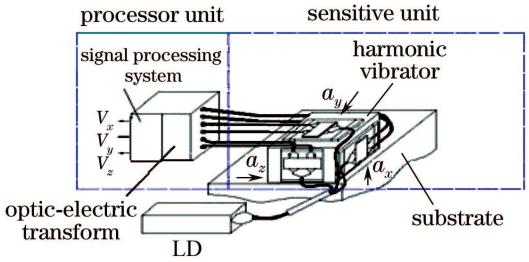

Fig. 5. Schematic of the three-component photoelastic waveguide accelerometer.

Figure 5 shows the schematic of the designed three-component photoelastic waveguide accelerometer with combined structure. The horizontally polarized laser beam from LD is split into three beams which pass through three MZIs respectively. When an arbitrary-direction acceleration is forced on the substrate, the three MZIs can be affected by the acceleration a_x, a_y, and a_z, separately. After converting the variation of acceleration component into the optical phase shift, the light will be transmitted into external processor unit, and we can deal with it by differential process. In this way, we can obtain the relationship between voltage and the acceleration to be monitored.

According to Table 1, TSR of the designed three-component accelerometer is zero theoretically, but it is difficult to fabricate a multi-axis accelerometer with zero TSR. The error of TSR results from the misalignment of the accelerometer's actual sensitive axis from desired direction and the misalignment of the polarized beam axis from the stress direction. The TSR of the accelerometer is studied by detecting the frequency spectrum.

The prototype accelerometer to be characterized is fixed onto the top of a mechanical vibrator which provides a simulating acceleration signal, as shown in Fig. 6. A spectrum analyzer is used to record the frequency spectrum. The sensitivity of the accelerometer as a function of vibration frequency is demonstrated in Fig. 7. The acceleration is in the vertical direction of light axis (a_z). The cross-axis sensitivity is lower than the on-axis sensitivity, and the corresponding resonance frequency is about 3.5 kHz, TSR = 0.1 (frequency range: 150 − 3000 Hz). It can be seen that the accelerometer has a good frequency responding characteristic when the frequency is below 3 kHz, which accords with the operation frequency in high-accuracy seismic exploration.

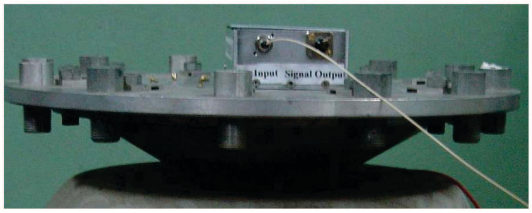

Fig. 6. Photograph of the accelerometer on the mechanical vibrator.

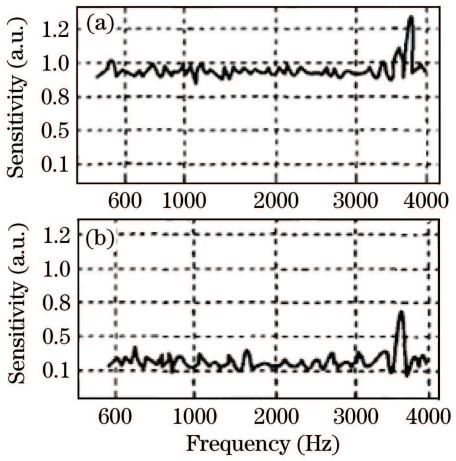

Fig. 7. (a) On-axis sensitivity and (b) cross-axis sensitivity versus vibration frequency for the acceleration in the vertical direction of light axis.

In conclusion, a novel three-component hybrid-integrated optical accelerometer based on $LiNbO_3$ photoelastic waveguide is presented. The cross-axis sensitivity to acceleration is a very important parameter for three-component accelerometer. We design the three-component hybrid-integrated optical accelerometer which shows a linear broad working frequency range. This accelerometer can be employed to monitor or accurately measure vibrations in various areas such as seismic measurement in geophysical survey.

This work was supported by the National Natural Science Foundation of China (No. 40774067) and the Applied Basic Research Program of Sichuan Province (No. 07JY029-135).

References

1. A. Llobera, J. A. Plaza, I. Salinas, J. Berganzo, J. Garcia, J. Esteve, and C. Domínguez, Sensors and Actuators A **110,** 395 (2004).
2. X. Kang, E. Dong, A. Qiu, and X. He, Acta Opt. Sin. (in Chinese) **26,** 202 (2006).
3. N. Zeng, C. Z. Shi, M. Zhang, L. W. Wang, Y. B. Liao, and S. R. Lai, Opt. Commun. **234,** 153 (2004).
4. S. Jia, W. Kong, and J. Yang, Acta Opt. Sin. (in Chinese) **27,** 1494 (2007).
5. H. Luo, S. Xiong, Y. Hu, and M. Ni, Chinese J. Lasers (in Chinese) **32,** 1382 (2005).
6. B. Wu, C. Chen, G. Ding, D. Zhang, and Y. Cui, Opt. Eng. **43,** 313 (2004).
7. M. Bozzetti, G. Calo, A. D'Orazio, M. De Sario, L. Mescia, V. Petruzzelli, and F. Prudenzano, in *Proceedings of ICTON Mediterranean Winter Conference (ICTON-MW) 2007* 1 (2007).
8. H. Pang, P. LiKamWa, and H. J. Cho, in *Proceedings of 5th IEEE Conference on Sensors* 1489 (2006).
9. P. V. Lambeck and H. Hoekstra, in *Proceedings of LEOS 2003* **2,** 967 (2003).
10. D. En, C. Chen, Y. Cui, and G. Ding, Chinese J. Lasers (in Chinese) **32,** 399 (2005).
11. C. Chen, D. Zhang, G. Ding, and Y. Cui, Appl. Opt. **38,** 628 (1999).
12. C. Chen, B. Wu, G. Ding, and Y. Cui, Proc. SPIE **4919,** 1 (2002).